

PREDICTING DEFORMATIONS IN ALUMINUM OVERLAP JOINT PRODUCED BY FSW PROCESS

The goal of the work was to develop model of Friction Stir Welding process that predicts deformations of the joined components based on the specified heat input. In the analyzed case two overlapping aluminum sheets were welded. The top sheet had the thickness of 1.0 and the bottom sheet had the thickness of 0.6 mm. The model used Finite Element Method. Thermal mechanical coupled formulation was chosen. The heat input was estimated based on the temperature measurements in the selected points along the welding line. Heat source was calibrated to match the numerically calculated and experimentally measured thermal cycles. The calculated field of displacements in direction perpendicular to the sheet surface was selected to compare the numerical results with the actual geometry of welded sheets. The model achieved the satisfying accuracy with respect to the qualitative description of the deformations.

Keywords: finite element method, friction stir welding, deformations, thin aluminum sheets, thermal cycles.

1. Introduction

Friction Stir Welding, FSW, is a solid state joining technology [1]. The process of joining involves heating and mixing a material at an interface between components. Both heating and mixing is produced by a rotating tool. FSW is applied in various industries [2]: aerospace (fuel tanks), civil aviation (joining stiffeners and skin), automotive (rim wheels, chassis), railway (double skin frameless structure), maritime (ship building panels). There are also variants of FSW technology that allow for making spot welds: Friction Stir Spot Welding, FSSW, produces spot weld with an exit hole [3], Refill Friction Stir Spot Welding, RFSSW, produces spot welds without an exit hole [4]. Most of research into FSW processes focus on joining components thicker than 1 mm [5,6]. Relatively few works discuss joining components having thickness of 1 mm or lower. Similarly, the majority of FSW application involves aluminum alloys, however new applications for steels [7] and titanium alloys [8] emerge that are alternative to the existing welding technologies [9,10].

There are many works describing numerical models of FSW process. Most of them focus on physics of heat generation and impact of tool geometry on temperature field. This task is very complicated since there is no agreement on the type of law to describe material behavior at high temperatures and at high strain rates [11]. Hamilton [12] and Uygur [13] used heat model calculating heat flux from friction and plastic deformation. The plastic deformation heat was calculated based on Johnson-Cook material model. The energy formulation showed good agreement with experimental data for aluminum 1050 and AA6061-T6.

Leśniewski [14] analyzed the influence of friction coefficient on heat generation. It was found out that the good results are obtained for friction models in which friction coefficient has peak value at 200°C and drops at higher temperatures. Lacki [15] investigated the impact of tool geometry on heat production and flash formation during FSSW process. Thermo-mechanical model was assumed. The heat was generated as a result of friction between contact surfaces. Buffa [16] and Fratini [8,17] developed hybrid model of FSW process. In the first stage they used rigid-visco-plastic formulation in order to calculate temperature distribution. Subsequently they used temperature distribution from the first stage and imposed it on thermal-elastic-plastic model. The result of the calculations in the second stage was stress field.

There are virtually no works describing numerical models that predict deformations of sheets due to FSW process. The aim of this paper is to fill this gap. The principles of deformation simulation for FSW process are the same as in the case of conventional welding technologies [18,19]. The heat source model calibrated based on experimental measurements causes changes of strains and stresses in the mechanical part of the model. These models ignore the physics of heat generation.

2. Experimental research

In order to calculate sheet deformations in response to heat input from the tool and assess the model accuracy it is necessary to measure thermal cycles in the sheets during welding. Thermal cycles present the dependence of temperature on time in

* CZEŃSTOCHOWA UNIVERSITY OF TECHNOLOGY, FACULTY OF CIVIL ENGINEERING, 69 DĄBROWSKIEGO STR., 42-201 CZEŃSTOCHOWA, POLAND

Corresponding author: konrad.adamus@gmail.com

a point. During the welding process two aluminum 2xxx sheets were joined, the top sheet had the thickness of 1.0 mm and was made of aluminum 2024 T3, the bottom sheet had the thickness of 0.6 mm and was made of aluminum D16 UTW. Aluminum D16 is the Russian counterpart of aluminum 2024. The scheme of the resultant FSW joint and the FSW process is presented in Fig. 1. The rotating tool plunges into the sheets from the top. Subsequently it moves along the welding trajectory and stirs the material at the interface between the sheets. The rotational speed was 2000 revolutions per minute. The welding speed was 1.65 mm/s. The tool pin had the conical geometry.

Fig. 2 presents the clamping device used for fixing the sheets during welding. Two flat steel bars positioned parallel to the welding line immobilize the sheets and prevent their motion. The FSW tool travels between these bars.

The macrostructure of the overlap joint in the cross-section normal to the welding line is presented in Fig. 3. The bottom sheet is coated with pure aluminum layer. This layer has the white color in the macrostructure in Fig. 3. At the sides and at the bottom the grains of the parent material can be observed. In the center and at the top the fine grained region of recrystallized material can be seen. The recrystallization process was triggered by the heat input and high strain rates which in turn were caused

by the motion of the rotating FSW tool. This zone is referred to as thermos-mechanically affected zone, TMAZ. The aluminum coating between the top and the bottom sheet was interrupted inside the TMAZ. The coating material was moved from the advancing to the retreating side of the weld.

Fig. 4 presents the layout of the points, where temperature was measured. The measurement points were denoted with dots. Three of the points are located at the top sheet at the line parallel to the welding line. The distance from the line to the welding line is 9 mm. The fourth point was located between the sheets, under the welding line. Thermocouples were attached in the measurement points. The thermocouples attached to the parallel line can be reused multiple times. However, the thermocouple between the sheets needs to be replaced for each new weld. Even if the continuity of this thermocouple remains intact, it can't be released from the joint without its destruction.

Fig. 5 presents thermal cycles measured by the thermocouples. These thermal cycles correspond to the welding speed of 3.3 mm/s and rotational speed of 2000 rotations per minute. The peak temperature corresponding to thermocouple between the sheets is about 390°C. This peak temperature is typical of the tool used in the research. The same technique was used for other tools and the temperature of 500°C was registered. The

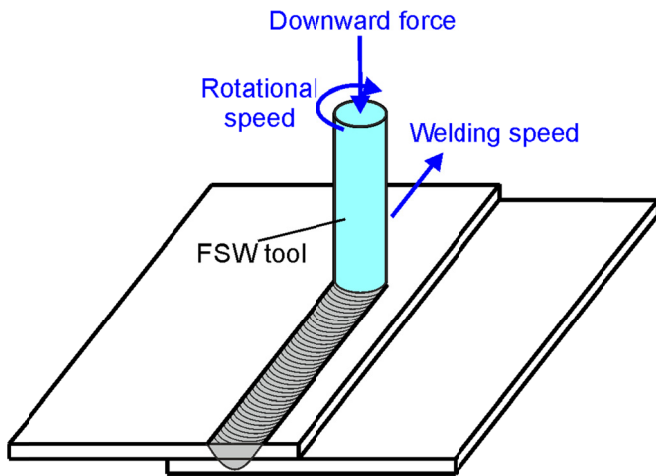


Fig. 1. Scheme of FSW joining of overlapping sheets

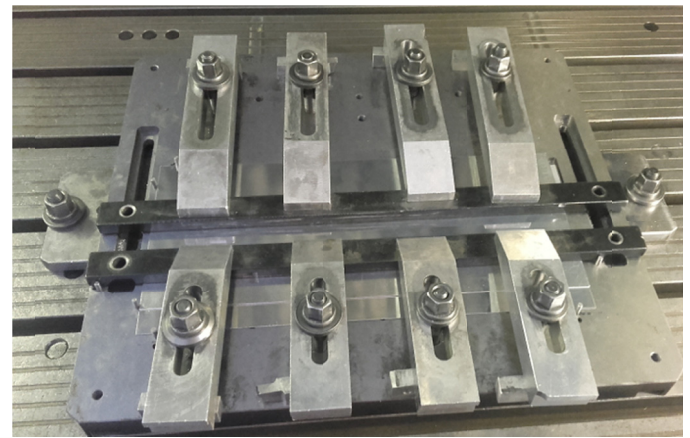


Fig. 2. The clamped aluminum sheets prepared for FSW process



Fig. 3. Macrostructure of FSW aluminum joint

low heat input of the tool used in research translates into lower sheet deformations. The peak temperature at the points along the line parallel to the welding line is about 140°C.

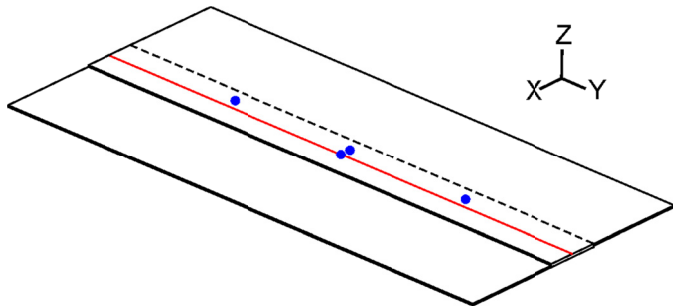


Fig. 4. The layout of temperature measurement points (dots) along welding line (middle line)

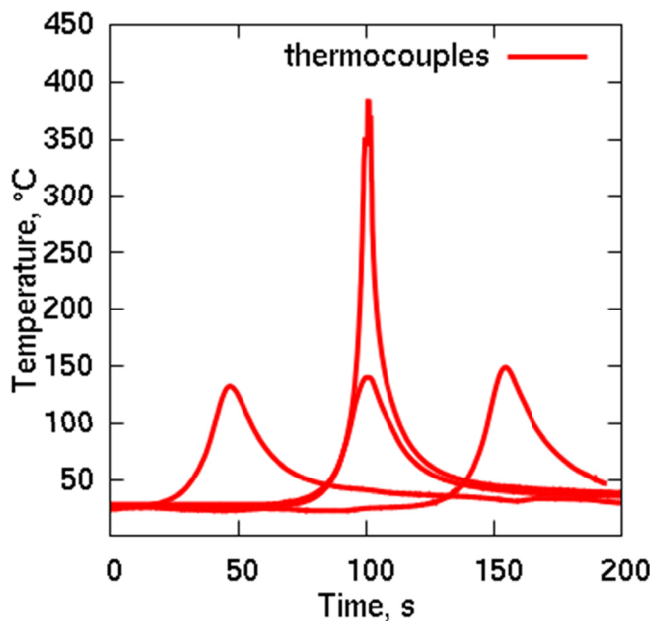


Fig. 5. Thermal cycles measured for FSW aluminum joint

3. Numerical model

The numerical model was built using ADINA which is based on Finite Element Method [20-22]. Thermo-mechanical coupled formulation was chosen.

Fourier-Kirchoff equation was applied to define heat propagation:

$$\frac{\partial T}{\partial t} = a \nabla^2 T + \frac{q_v}{\rho c_p} \quad (1)$$

where: T – temperature, a – thermal diffusivity, ρ – density, c_p – specific heat, q_v – efficiency of inner volume heat source. Thermal diffusivity is defined as:

$$a = \frac{\lambda}{\rho c_p} \quad (2)$$

where: λ – thermal conductivity.

Thermo-elastic-plastic material was described by constitutive equation:

$${}^t\sigma_{ij} = {}^tC_{ijrs}^E \left({}^t e_{rs} - {}^t e_{rs}^P - {}^t e_{rs}^{TH} \right) \quad (3)$$

where: ${}^t\sigma_{ij}$ – stress tensor at time t , ${}^tC_{ijrs}^E$ – elasticity tensor at temperature corresponding to time t , ${}^t e_{rs}$ – total strain tensor at time t , ${}^t e_{rs}^P$ – time independent plastic strain tensor at time t , ${}^t e_{rs}^{TH}$ – thermal strain tensor at time t .

Thermal strains are calculated based on thermal expansion coefficient and temperature in nodes. Thermal conductivity, specific heat capacity, strain-stress relationships are temperature dependent. Plastic strains are calculated based on von Mises plasticity criterion:

$${}^t f_y = \frac{1}{2} {}^t s \cdot {}^t s - \frac{1}{3} {}^t \sigma_y^2 \quad (4)$$

where: ${}^t s$ – deviatoric stress tensor at time t , ${}^t \sigma_y$ – yield stress. The associated flow rule is defined as:

$$de_{ij}^P = d\lambda {}^t s_{ij} \quad (5)$$

where: $d\lambda$ – plastic multiplier, $d\lambda > 0$.

Surface heat source consisting of two parts was applied, Fig. 6. Heat flux can be assigned independently to the external (annulus) and internal (disk) parts. Within each part heat flux is constant. The heat is transported into three-dimensional elements whose sides are within the heat source. The external diameter of the heat source was equal to the diameter of the tool shoulder. Changing the ration of heat transported through the internal and external parts changes the ratio of peak temperatures between the points at the line parallel to the welding trajectory and the points under the welding line, Fig. 5. The power of the heat source was set to 200 W

Calibration of the thermal model has to take into account heat exchange with clamping devices. Convective heat transfer was applied to the sheet boundaries in order to simulate heat exchange between the sheets and the surrounding air as well as the sheets and the fixtures. The rate of convective heat exchange was defined by the equation [23]:

$$q = h(T_S - T_F) \quad (6)$$

where: q – heat flux, h – convective heat transfer coefficient, T_S – the temperature of an external sheet surface, T_F – the temperature of fluid. The application of convective heat transfer to the description of the heat transfer between welded objects and fixtures was described in [11]. In that case the convective heat transfer coefficient describes the heat exchange between two solid bodies and the temperature difference represents the difference between the temperatures of the welded objects and the temperature of the fixtures. The studies performed by Zahedul [24] indicate that high value of convective heat transfer coefficient, 4000 W/m², underestimate peak temperature and low value, 0 W/m², result in peak temperature above melting point. The value of 1000 W/m² was suggested. This is in line with research of Bosetti [25]. According to Bosetti heat transfer

coefficient is equal to 1000 W/m^2 for pressure of 5 MPa and 1500 W/m^2 for pressure of 10 MPa. The pressure produced by the clamping device was not measured, the convective heat transfer coefficient was experimentally selected and was set to 1200 W/m^2 . The surfaces corresponding to heat exchange with clamping device were denoted with dark gray color in Fig. 7. For these surfaces, convective heat transfer coefficient was set to 1200 W/m^2 . For the other surfaces, denoted with light gray color, convective heat transfer coefficient was set to 10 W/m^2 . It corresponds to the heat exchange with air.

The clamping device was modelled using two-dimensional spring elements. One end of the spring is attached to a node and the other end is fixed. The spring stiffness changes in time to represent releasing the sheets after the welding end. The spring elements were attached to nodes at contact surfaces between flat steel bars and sheets. These surfaces were denoted with dark gray color in Fig. 7.

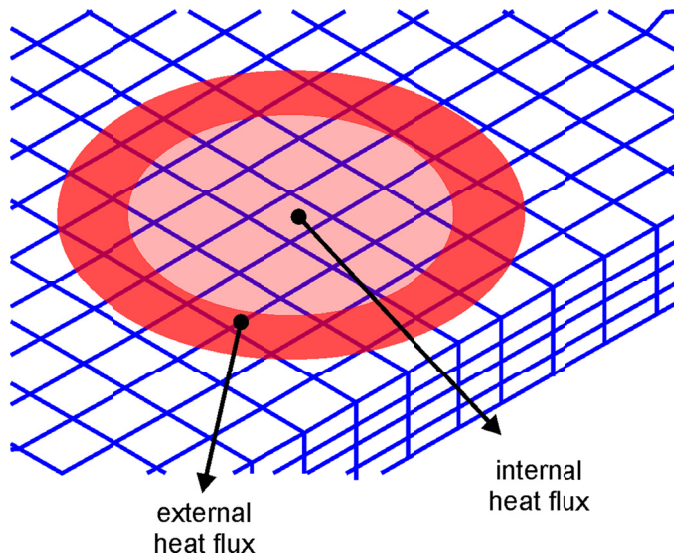


Fig. 6. Scheme of a heat source

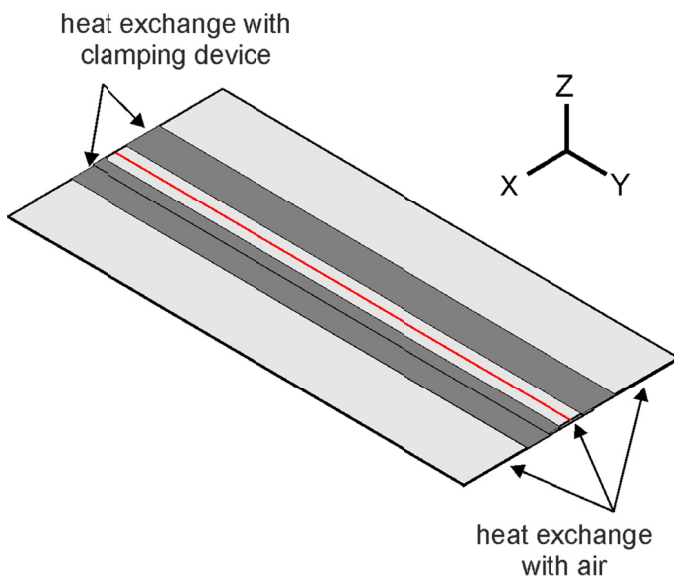


Fig. 7. Heat exchange with surrounding

4. Analysis of the results

The heat source was calibrated to achieve match between numerically calculated and experimentally measured thermal cycles. Fig. 8 presents the comparison of the numerical and experimental results. It can be seen that there is a good match. The only discrepancy occurs during cooling of the material. The actual sheet cools more slowly than material in the numerical model.

Fig. 9 presents the comparison of macrostructure (left side) and calculated temperature distribution during heat sources pass (right side) in the cross-section perpendicular to the welding line. The recrystallized material in TMAZ corresponds to the temperatures above 310°C in the simulation. The application of the surface heat sources comprising annulus and disk, each having different heat flux assigned, allows for achieving isotherms that have shape similar to the outline of TMAZ. Isotherms in the center have triangular shape. They are wide at the top and narrow at the bottom. Moving further away from the weld center temperature tends to have similar values in the whole thickness of the sheets. The isotherms change into almost vertical line.

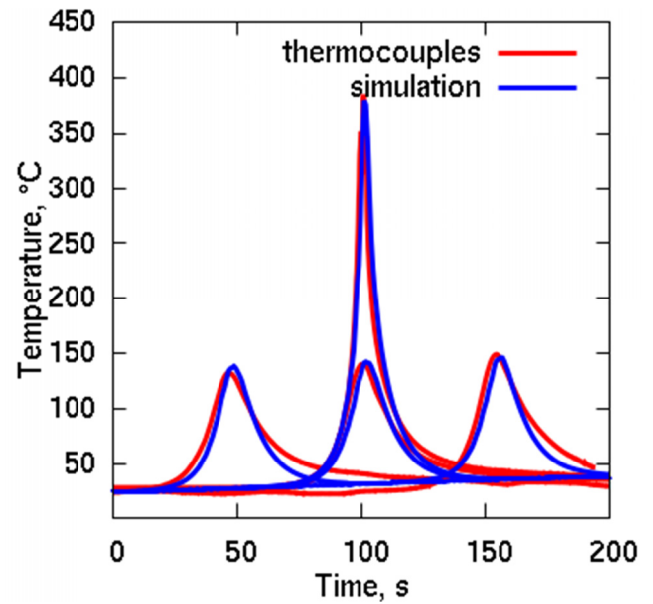


Fig. 8. Comparison of numerically calculated and experimentally measured thermal cycles

In order to assess the accuracy of the model the deformations of the actual sheets were compared with the calculated displacements in the direction of Z axis, Fig. 10. Part (a) of Fig. 10 presents FSW joint fixed at its corners. Each of the corners is situated at the block of material. Each of the blocks has the same thickness. Additionally, each of the corners is pressed by steel rings. The same setup was applied in the simulation. The corners of the weld were fixed by spring elements acting in Z direction. Effectively, both the corner nodes in the simulation and actual sheet corners were at the same height. Additionally, the sheets were allowed to freely deform in direction below and above the corners.

It can be seen that the bottom sheet is bent in upward direction. The Z-displacement of its middle part was equal to 6.1 mm



Fig. 9. Comparison of macrostructure and calculated temperature field in the joint cross-section

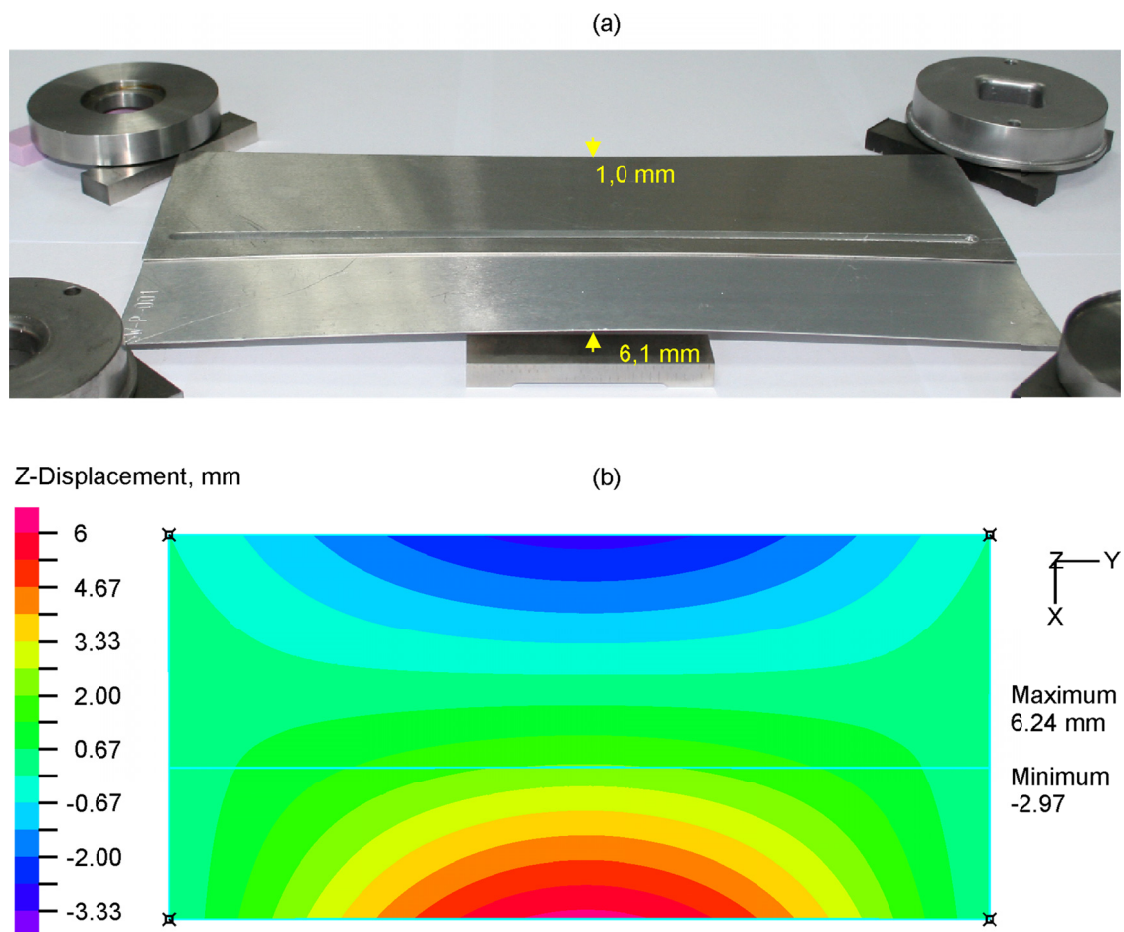


Fig. 10. Comparison of: (a) welded sheets, (b) calculated Z-displacement distribution

and was measured relative to the block of material as denoted in Fig. 10 (a). In a similar way the bending of the top sheet was measured. The Z-displacement of the middle part of the top sheet was in downward direction and was equal to 1 mm. Fig. 10 (b) presents the calculated Z-displacement field. The maximum Z-displacement was equal to 6.24 mm and was located in the middle part of the bottom sheet. The Z-displacement in downward direction equals 2.97 mm and was located in the middle part of the top sheet.

5. Conclusions

Based on the carried out research the following conclusions can be drawn:

- It is possible to create thermo-mechanical model of FSW process predicting joint distortion in response to the heat produced by FSW tool.
- The model requires calibration of both: heat source representing the action of the FSW tool and equivalent con-

vective coefficient representing the heat exchange with clamping device.

- The equivalent convective coefficient was assessed to be about 1200 W/m^2 .
- The suggested heat source model allows for achieving good match between numerically calculated and experimentally measured thermal cycles.
- There is good qualitative agreement between numerically calculated and experimentally measured sheet deformations. The bottom sheet is bent upward. The top sheet is bent downward. The degree of the bending is higher in the bottom sheet.
- There is good quantitative agreement in the degree of bending in the bottom sheet. The actual degree of bending is 6.1 mm. The calculated degree of bending is 6.24 mm.
- The degree of bending in the top sheet is overestimated. The actual degree of bending is 1 mm. The calculated degree of bending is 2.97 mm.

Acknowledgements

Financial support of The National Centre for Research and Development, European Union, PZL Mielec A Sikorsky Company in the framework of European Regional Development Fund Project “Advanced techniques for the fabrication of airframe structures using innovative friction stir welding (FSW) technology”, Nr INNOLOT/I/4/NCBR/2013 is gratefully acknowledged.

REFERENCES

- [1] R.S. Mishra, P.S. De, N. Kumar, Friction stir welding and processing: Science and engineering, Springer (2014).
- [2] A. Amini, P. Asadi, P. Zolghadr, Friction stir welding applications in industry, in: M. K. Besharati Givi, P. Asadi (Eds.), Advances in friction stir welding and processing, Woodhead Publishing (2014).
- [3] M.K. Kulecki, Arch. Metall. Mater. **59** (1), 221-224 (2014).
- [4] A. Derlatka, P. Kasza, Adv. Mat. Res. **1020**, 151-157 (2014).
- [5] K. Krasnowski, P. Sędek, M. Łomozik, A. Pietras, Arch. Metall. Mater. **56** (4), 965-973 (2011).
- [6] B. Rams, A. Pietras, K. Mroczka, Arch. Metall. Mater. **59** (1), 385-392 (2014).
- [7] A.M. El-Batahgy, T. Miura, R. Ueji, H. Fujii, Mater. Sci. Eng. A, **651**, 904-913 (2016).
- [8] L. Fratini, F. Micari, G. Buffa, V. F. Ruisi, CIRP Ann. Manuf. Techn. **59** (1), 271-274 (2010).
- [9] J. Adamus, P. Lacki, M. Motyka, Arch. Civ. Mech. Eng. **15** (1), 42-47 (2015).
- [10] J. Adamus, M. Motyka, Key Eng. Mater. **639**, 339-346 (2015).
- [11] A. Simar Y. Brechet, B. de Meester, A. Denquin, C. Gallais, T. Pardeon, Prog. Mater. Sci. **57** (1), 95-183 (2012).
- [12] C. Hamilton, A. Sommers, S. Dymek, Int. J. Mach. Tool. Manu. **49** (3-4), 230-238 (2009).
- [13] I. Uygur, Arch. Metall. Mater. **57** (1), 53-60 (2012).
- [14] J. Leśniewski, A. Ambroziak, Arch. Civ. Mech. Eng. **15** (1), 142-150 (2015).
- [15] P. Lacki, Z. Kucharczyk, R.E. Śliwa, T. Gałaczyński, Arch. Metall. Mater. **58** (2), 595-599 (2013).
- [16] G. Buffa, A. Ducato, L. Fratini, Finite Elem. Anal. Des. **47** (4), 470-476 (2011).
- [17] L. Fratini, G. Macaluso, S. Pasta, J. Mater. Process. Tech. **209** (15-16), 5465-5474 (2009).
- [18] Z. Saternus, W. Piekarska, M. Kubiak, T. Domański, L. Sowa, Procedia Eng. **136**, 95-100 (2016).
- [19] W. Piekarska, K. Rek, Procedia Eng. **177**, 182-187 (2017).
- [20] K.J. Bathe, Finite Element Procedures, Klaus-Jurgen Bathe, Cambridge (2006).
- [21] ADINA, ADINA Theory and Modeling Guide Volume I: ADINA, ADINA R& D, Inc., Watertown (2016).
- [22] ADINA, ADINA-T Theory and Modeling Guide Volume II: ADINA Heat Transfer, ADINA R& D, Inc., Watertown (2016).
- [23] P. Nithiarasu, R.W. Lewis, K.N. Seetharamu, Fundamentals of the finite element method for heat and mass transfer, John Wiley & Sons, Ltd, Chichester (2016).
- [24] M. Zahedul, H. Khandkar, J.A. Khan, J. Mater. Process. Manu. Sci. **10**, 91-105 (2001).
- [25] P. Bosetti, S. Bruschi, T. Stoehr, J. Lechler, M. Merklein, Int. J. Mater. Form. **3** (1), 817-820 (2010).